INSTITUTE OF PHYSICS PUBLISHING JOURNAL OF PHYSICS B: ATOMIC, MOLECULAR AND OPTICAL PHYSICS

J. Phys. B: At. Mol. Opt. Phys. **36** (2003) 235–246 PII: S0953-4075(03)53629-X

The effects of coupling to the target continuum on the electron-impact excitation of Li^+

C P Ballance[1], N R Badnell[2], D C Griffin[1], S D Loch[3] and D M Mitnik[1]

[1] Department of Physics, Rollins College, Winter Park, FL 32789, USA
[2] Department of Physics, University of Strathclyde, Glasgow G4 0NG, UK
[3] Department of Physics, Auburn University, Auburn, AL 36849, USA

Received 9 September 2002, in final form 18 November 2002
Published 7 January 2003
Online at stacks.iop.org/JPhysB/36/235

Abstract

We have investigated the effects of coupling to the continuum and high bound states on the electron-impact excitation of He-like Li^+ using the R matrix with pseudostates (RMPS) method. Previous studies on this ion have focused on transitions from the ground state to the $n = 2$ terms. In this work, we have determined collision strengths between all 19 terms through $n = 4$. We present the results of two RMPS calculations with different numbers of pseudostates in order to study the convergence of the collision strengths with the size of the pseudostate expansion. In addition, we compare the RMPS collision strengths with the results of an R-matrix calculation without pseudostates in order to determine the influence of the continuum coupling as a function of electron energy. As one might expect, coupling to the target continuum has quite large effects on the collision strengths for excitation to the $n = 3$ and 4 terms at energies above the ionization limit. However, we find that these effects are also significant for excitation to the $n = 2$ terms and that they persist down to energies just above the excitation thresholds. The experience gained from this work will allow us to pursue similar studies in more complex target systems. Furthermore, the results of our largest RMPS calculation provide the most complete and accurate set of excitation data for this ion, which is of significant importance to research in controlled nuclear fusion.

(Some figures in this article are in colour only in the electronic version)

1. Introduction

Fast Li-beam diagnostic analyses in various controlled nuclear fusion experiments require high-calibre electron-impact excitation data for the entire Li isonuclear sequence. Work on neutral Li has been completed by Griffin *et al* (2000). The present study considers electron-impact excitation of Li^+, while the results for Li^{2+} have also been completed and will be reported soon.

 © 2003 IOP Publishing Ltd Printed in the UK

In recent years, the R matrix with pseudostates (RMPS) method has been successfully used to represent the effects of coupling to the target continuum and the high Rydberg states (Bartschat *et al* 1996, Badnell and Gorczyca 1997). Experience gained from a hydrogen study (Anderson *et al* 2000) showed that pseudostates were essential to represent the effect of coupling to the target continuum above the ionization limit. Furthermore, RMPS calculations in the Li-like ions Be^+ (Bartschat and Bray 1997), B^{2+} (Marchalant *et al* 1997), C^{3+} and O^{5+} (Griffin *et al* 2000) demonstrate that these effects are not only important above the ionization limit but are also present at energies just above the excitation thresholds. One of the significant challenges for collisional atomic physicists is to move beyond hydrogenic and alkali targets and investigate the effects of the target continuum on excitation in more complex species. However, even in He-like systems the presence of both singlet and triplet terms in the pseudostate basis scales the calculation accordingly.

There have been a number of Li^+ excitation studies. For example, Christensen and Norcross (1984) carried out distorted-wave (DW) and a five-state close-coupling (CC) calculations for the excitation to the $n = 2$ terms of this ion. Griffin and Pindzola (1990) determined the total and differential excitation cross sections to the $n = 2$ terms from DW, five-state CC and 11-state CC calculations. Berrington and Nakazki (1991) carried out five-state, 11-state and 19-state R-matrix calculations for this ion. They focused on excitation to the $n = 2$ terms, though they did present collision strengths to the $n = 3$ terms at a single electron energy. Subsequently, Brown *et al* (1999) applied an RMPS method for excitation to the $n = 2$ terms in Li^+. They used spectroscopic states for all terms through $n = 3$ and a limited number of Sturmian-type orbitals (rather than the more complete set of Laguerre pseudo-orbitals used in the present study) to represent the target continuum. They reported that their pseudostate expansion was limited by the numerical instability of their analytic Schmidt orthogonalization procedure, a problem that we are able to circumvent by employing the method of Badnell and Gorczyca (1997). This study endeavours to determine the extent and type of pseudostate basis required to accurately model excitation from the first excitation threshold to approximately 10 Ryd. The complete set of effective collision strengths from our most extensive calculation, as well as radiative rates for all dipole transitions, have been made available on the Internet at the Oak Ridge National Laboratory (ORNL) Controlled Fusion Atomic Data Centre (CFADC).

The remainder of the paper is structured as follows. The next section describes our spectroscopic target basis as well as the range of pseudostate expansions employed to investigate the convergence of the collision strengths. In section 3, we analyse and compare our collision strengths and effective collision strengths for Li^+. In section 4, we summarize our work, discuss the accuracy of our results, and consider future studies using our RMPS method.

2. Target description

All target terms employed in this work were generated using AUTOSTRUCTURE (Badnell 1997). The spectroscopic orbitals (1s–4f) were determined using local potentials derived from Slater-type functions. The pseudo-orbitals were constructed from non-orthogonal Laguerre functions that were subsequently orthogonalized to the spectroscopic orbitals and to each other. The present energy levels are compared with previous work in table 1. We note that there is, in general, good agreement between our theoretical values and the experimental energies from the National Institute of Standards and Technology (NIST) Physical Reference Data[4]. The present wavefunctions used in the calculations provide energies that are accurate to within 0.5% or better of the observed values as illustrated in table 1.

[4] http://physics.nist.gov/PhysRefData.

Table 1. Energy-level (Ryd) comparisons with previous theoretical and experimental results. Christensen and Norcross (1984) give a range of values corresponding to three models while the Brown *et al* (1999) values are for their unadjusted data.

Index	Term	Christensen and Norcross (1984)	Brown *et al* (1999)	Present	NIST
1	$1s^2\ ^1S^e$	0.0000	0.0000	0.0000	0.0000
2	$1s2s\ ^3S$	4.3076–4.3441	4.2778	4.3261	4.3380
3	$1s2s\ ^1S$	4.4472–4.7260	4.4239	4.4996	4.4777
4	$1s2p\ ^3P$	4.4740–4.5032	4.4470	4.5021	4.5041
5	$1s2p\ ^1P$	4.5429–4.5792	4.5167	4.5938	4.5728
6	$1s3s\ ^3S$	—	4.9946	5.0600	5.0553
7	$1s3s\ ^1S$	—	5.0331	5.1032	5.0920
8	$1s3p\ ^3P$	—	5.0387	5.1043	5.0986
9	$1s3d\ ^3D$	—	5.0536	5.1225	5.1144
10	$1s3d\ ^1D$	—	5.0539	5.1232	5.1147
11	$1s3p\ ^1P$	—	5.0596	5.1305	5.1191
12	$1s4s\ ^3S$	—	—	5.2923	5.2852
13	$1s4s\ ^1S$	—	—	5.3093	5.2999
14	$1s4p\ ^3P$	—	—	5.3098	5.3025
15	$1s4d\ ^3D$	—	—	5.3172	5.3092
16	$1s4f\ ^3F$	—	—	5.3174	5.3094
17	$1s4f\ ^1F$	—	—	5.3174	5.3094
18	$1s4d\ ^1D$	—	—	5.3176	5.3093
19	$1s4p\ ^1P$	—	—	5.3206	5.3111

Our dipole radiative rates between the $n \leqslant 3$ terms are compared with values provided in the NIST database in table 2. The majority of these rates compare quite favourably with the NIST values (all of which are rated either A or B); this is especially true for the stronger transitions that agree to within 10% or better.

The three target models employed in this work are described in table 3. In this table, we denote the Laguerre pseudo-orbitals by $\bar{n}\bar{l}$. All terms within models a–c include only singly excited states. The eigenenergies of the doubly excited states are beyond the highest electron energy of 9.66 Ryd that was used in our collision calculations. Furthermore, the inclusion of doubly excited terms would lead to a stark increase in the number of $(N + 1)$-electron correlation terms in our CC expansion. Model a contains no pseudostates, but includes $n = 5$ spectroscopic terms; this provides an unbiased comparison with the $n = 4$ models that have a layer of pseudostates below the ionization threshold. Models b and c allow us to study the convergence of the pseudostate expansion.

The density and positions of these pseudostates are shown in figure 1. The layer of pseudostates below the ionization threshold is necessary to model the infinite number of bound states with $n \geqslant 5$ that are not included within our CC expansion. The continuum states above 5.556 Ryd are represented by the remainder of pseudostates, and they are closely clustered around the ionization threshold, with a more even distribution beyond that. The RMPS collision strengths are improved by ensuring that there is at least one singlet and one triplet pseudostate term with the same $\bar{l}$, below and above this limit. The number and position of the pseudostates in model c should be sufficient to achieve convergence in the calculated collision strengths at the highest energies considered in these calculations.

There are a number of advantages in retaining only spectroscopic terms with $n \leqslant 4$ in our RMPS calculations. The inclusion of the $n = 5$ terms would make the determination of an accurate structure for the $n \leqslant 4$ terms more difficult, since the ordering of these high terms

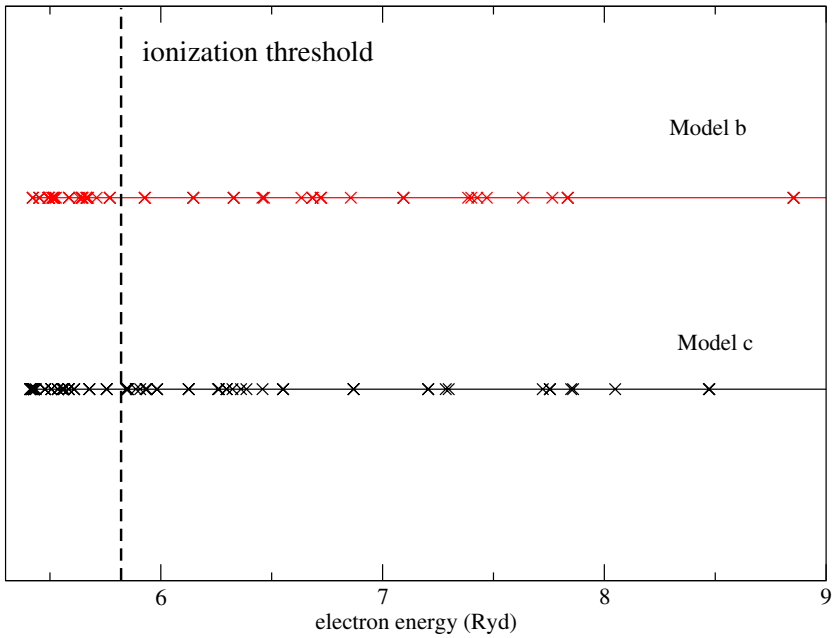

Figure 1. Pseudostate distribution across the ionization threshold for models b–c (see text for details). Model c has the more dense pseudostate distribution across the ionization threshold, which lies at 5.56 Ryd.

Table 2. Comparison of radiative rates with NIST values for all dipole-allowed transitions with $n \leqslant 3$.

Transition	Present	NIST	Transition	Present	NIST
1–5	2.65(10)[a]	2.56(10)	4–9	1.13(9)	1.12(9)
1–11	8.57(9)	7.79(9)	5–7	2.06(8)	2.04(8)
2–4	2.28(7)	2.76(7)	5–10	9.88(8)	1.01(9)
2–8	2.45(8)	2.88(8)	6–8	2.81(6)	3.54(6)
3–5	5.23(6)	5.18(6)	7–11	7.27(5)	7.10(5)
3–11	2.76(8)	2.82(8)	8–9	1.67(5)	1.10(5)
4–6	2.48(8)	2.85(8)	10–11	1.69(4)	3.98(3)

[a] $a(b) \equiv a \times 10^{b}$.

Table 3. Scattering models used for the electron-impact excitation of Li^{+}.

Model	Target terms	n	l	No of pseudo-orbitals	$\bar{n}$	$\bar{l}$
a	29	5	4	0	—	—
b[a]	19	4	3	48	5–9	0–5
c	19	4	3	82	5–11	0–5

[a] Model b omits the 9h pseudo-orbital.

is very sensitive to small changes in the 1s through 4f orbitals. Secondly, the inclusion of a real 5s orbital would increase the extent of the R-matrix inner region by over 30%, demanding more continuum orbitals to span the same energy range. Our largest calculation is already substantial, with 101 terms in the CC expansion and having $(N + 1)$-electron Hamiltonian matrices of rank up to approximately 17 000. Furthermore, the inclusion of the $n = 5$ real

terms would require an increase in the number of pseudostates if we are to maintain one layer of pseudostates below the ionization threshold. Again, this would further enlarge the size of our inner region $(N + 1)$-electron Hamiltonian.

3. Collision calculations

Modified versions of the R-matrix inner region suite of codes developed by Berrington *et al* (1995), and including the aforementioned orthogonalization procedure of Badnell and Gorczyca (1997), were used to generate all partial waves from $L = 0$ to 10. We employed 50 continuum basis orbitals to span the energy region between 0 and 18 Ryd, which is nearly twice the highest energy used in our collision calculations. Our largest RMPS calculation had 101 terms and a maximum of 321 LS resolved channels resulting in matrices of rank approximately 17 000. These cases benefit greatly from the parallel diagonalization of the inner region $(N + 1)$-electron Hamiltonian, as implemented in our parallel version of STG3 (Mitnik *et al* 2001). The non-exchange code of Burke *et al* (1992) was employed to generate the higher partial waves from $L = 11$ to 60. These high-L contributions were then topped-up for the dipole transitions using a method described by Burgess (1974). The non-dipole transitions were topped-up assuming a geometric series in L, using energy ratios and a special procedure to handle transitions between nearly degenerate levels, based on the degenerate limiting case (Burgess *et al* 1970).

The outer region calculation was carried out using a modified version of the unpublished code STGF (Seaton 1983). We used 3800 points (mesh $\approx$0.0004 Ryd) in the resonance region below the ionization threshold, but less than 100 above. For charged species, in which the Rydberg series can straddle target thresholds and affect low temperature effective collision strengths, we must address the question of resonance resolution. We filtered our final collision strength file to remove those points where the collision strengths differed from adjacent points by a predetermined value. We had only to remove a handful of points at all energies and for all transitions when this value was set at 10, indicating that our resonant structure was well resolved.

In figure 2, the collision strengths for the dipole-allowed transitions from the Li^+ ground state are shown in the context of our three models. Continuum coupling effects are evident in the first dipole transition to 1s2p ^{1}P (upper plot) and become significant, especially at higher energies; at 9 Ryd the collision strength from model a is about 1.40 times that from model c. It is rather surprising that these effects are this large for a transition to an $n = 2$ term. Furthermore, they persist down to low energies. This is illustrated in figure 3 which focuses on the collision strength for the transition to the 1s2p ^{1}P term below the ionization limit; model a (dotted curve) is consistently 10–15% higher than models b and c in this low-energy region. Model b (dashed curve) agrees remarkably well with model c (solid curve) up to 5.1 Ryd, before a slight separation emerges. Furthermore, we see from the top plot in figure 2 that the differences between the collision strengths for this transition calculated from models b and c are quite small up to 9 Ryd, where they differ by less than 10%.

By referring to the lower two plots in figure 2, we see that as we progress along this dipole-allowed sequence of transitions, the effects of coupling to the target continuum are more acutely felt as the final states approach the ionization limit. For example, at 9 Ryd, the collision strength for excitation to the 1s3p ^{1}P term from model a is about 1.9 times that from model c, while for excitation to the 1s4p ^{1}P term, the collision strength from model a is about 2.4 times that from model c. We also see from the lower two plots that the differences between the two pseudostate models are larger for excitation to the $n = 3$ and 4 terms. Table 4 complements figure 2 and gives the numerical values within all three models at 1 Ryd intervals

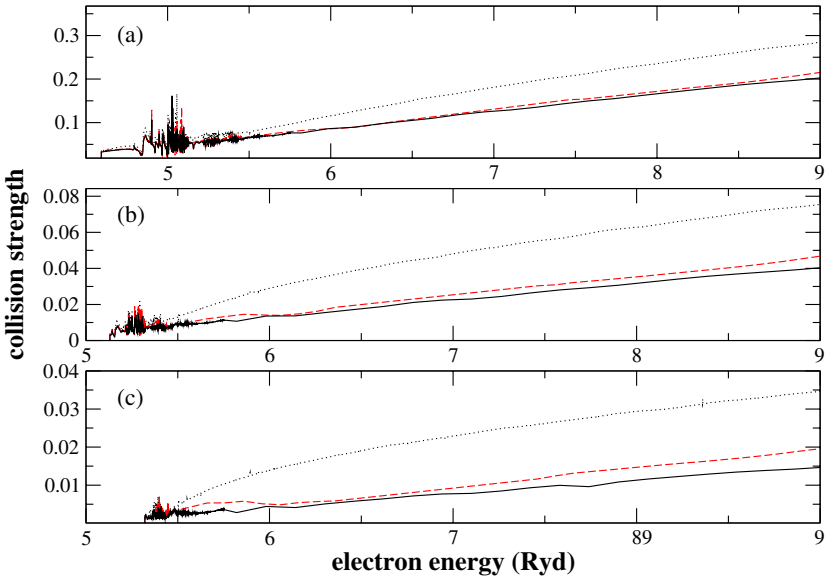

Figure 2. Collision strengths for the dipole-allowed transitions from the ground state, determined from models a–c. Model a is represented by the dotted curve, model b by the dashed curve and model c by the solid curve. (a) Excitation to 1s2p ^{1}P, (b) excitation to 1s3p ^{1}P, and (c) excitation to 1s4p ^{1}P.

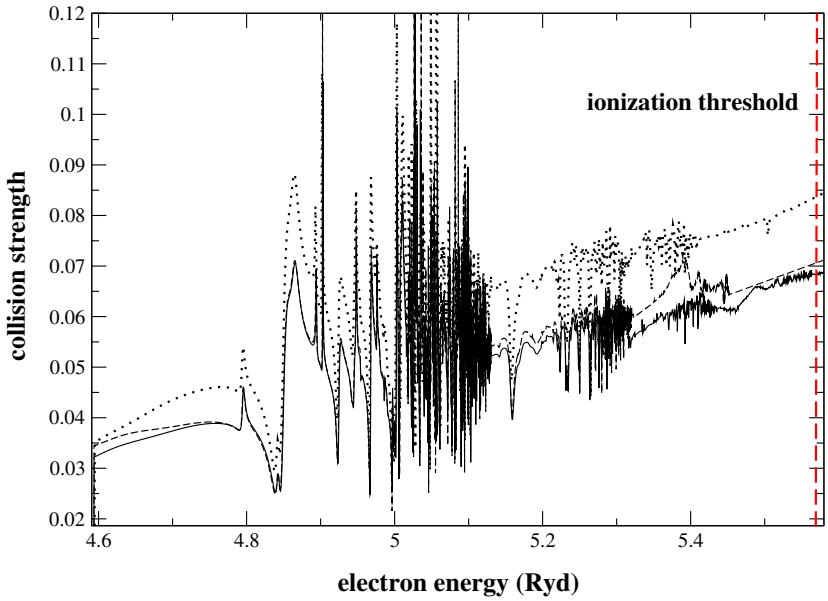

Figure 3. Collision strengths for the first dipole-allowed transition 1s^2 ^{1}S–1s2p ^{1}P below the ionization threshold, determined from models a–c.

above the ionization limit. There is good agreement between models b and c up to 7 Ryd for all transitions. At 9 Ryd, the collision strengths for the 1s^2 ^{1}S–1s4p ^{1}P transition differ at most by 25% between these two pseudostate models. Thus, although we have not yet reached

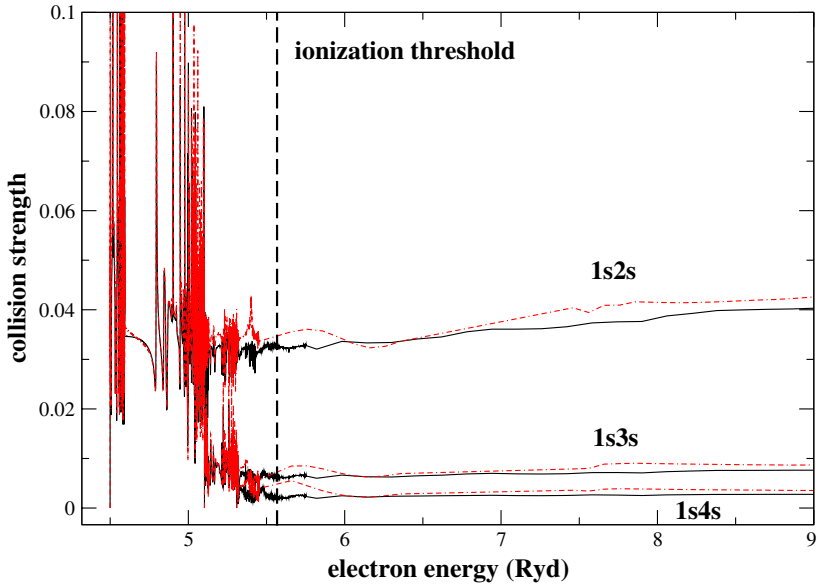

Figure 4. Collision strengths for spin-allowed monopole transitions from the ground term determined from models b and c.

Table 4. Collision strengths for the dipole-allowed transitions from the ground state for models a–c.

	$1s^2\ ^1S$–$1s2p\ ^1P$			$1s^2\ ^1S$–$1s3p\ ^1P$			$1s^2\ ^1S$–$1s4p\ ^1P$		
Energy (Ryd)	a	b	c	a	b	c	a	b	c
6.0	0.115	0.086	0.086	0.029	0.014	0.014	0.014	0.005	0.004
7.0	0.181	0.130	0.126	0.048	0.025	0.023	0.023	0.009	0.008
8.0	0.235	0.171	0.166	0.063	0.035	0.032	0.029	0.014	0.011
9.0	0.285	0.214	0.202	0.076	0.046	0.040	0.035	0.020	0.015

convergence in the pseudostate expansion, we would expect that even for the $1s^2\ ^1S$–$1s4p\ ^1P$ transition at the higher electron energies, model c should be within about 15% of a fully converged pseudostate calculation.

In our non-pseudostate R-matrix calculation, coupling to the $n = 5$ terms is included explicitly. The ideal result for our $n = 4$ spectroscopic plus pseudostate models is that the pseudostates below the ionization limit will account for coupling to these and higher terms; however, we might expect a slight inflation in the collision strength across the ionization limit. This effect appears in the form of oscillations in the collision strengths for the three monopole transitions $1s^2\ ^1S$–$1s\ ns\ ^1S$ shown in figure 4 in the energy range across the ionization limit. This is most pronounced in model b; however, it is nearly eliminated by the denser mesh of pseudostates just above the ionization limit in model c.

The RMPS results of Brown *et al* (1999) are in good agreement with the collision strengths determined from our most elaborate RMPS calculations, although they only presented excitations from the ground state to the $n = 2$ terms. In the case of the first dipole-allowed transition from the ground state at 9 Ryd, we obtain agreement with their value of the collision strength to within 3%. In the case of the first spin-allowed monopole transition from the ground

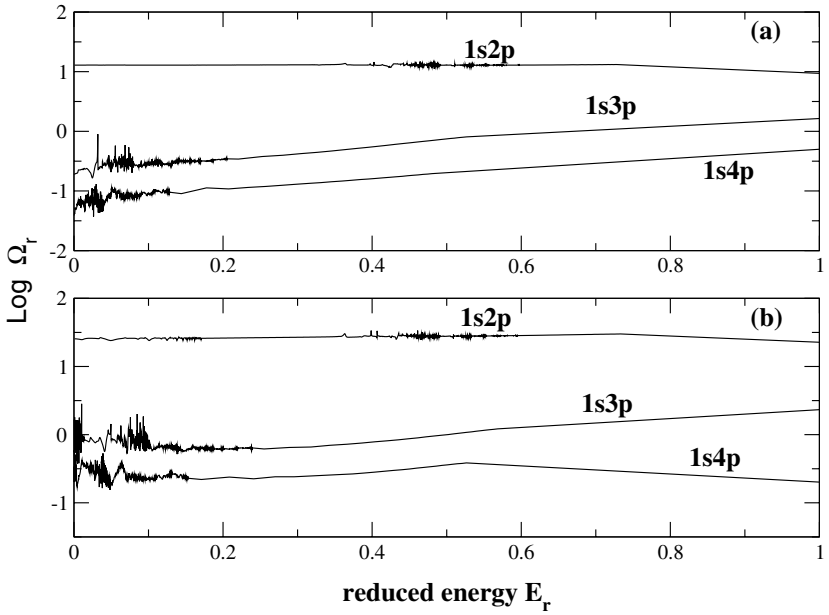

Figure 5. Reduced dipole-allowed collision strengths from the (a) 1s2s ^{1}S and (b) 1s2s ^{3}S terms, as a function of reduced energy (see text for details).

state at this same energy, we agree with their collision strength value of 0.04. It should be noted that in our RMPS calculations we include spectroscopic $n = 4$ terms in our CC expansion, whereas the most elaborate model of Brown *et al* used a set of $n = 4$ pseudo-orbitals to improve the structure of the target as well as the $(N + 1)$-electron correlation terms.

It is our intention that Maxwell-averaged effective collision strengths derived from our data be used in plasma modelling. However, the determination of effective collision strengths over a wide range of temperatures requires that our calculated collision strengths be extended to higher energies. In figure 5, we show plots of reduced collision strengths ($\Omega_{\rm r}$) for the dipole-allowed transitions from the 1s2s ^{3}S and 1s2s ^{1}S metastable terms as a function of reduced energy ($E_{\rm r}$), as introduced by Burgess and Tully (1992) regarding $E_r = 1 - 1/\ln(E_j/E_{ij} + {\rm e})$ and $\Omega_{\rm r} = \Omega/\ln(E_j/E_{ij} + {\rm e})$. Here, E_j corresponds to the scattered-electron energy and E_{ij} the energy separation between terms i and j.

In the case of dipole-allowed transitions, the infinite-energy reduced collision strength is given by the Bethe approximation and it reduces simply to $4S/3$, where S is the line strength. Burgess *et al* (1997) extended this work to include the high-energy Born limits for the optically forbidden (spin-allowed) transitions. Recently, Badnell and Thomas (see Whiteford *et al* 2001) implemented and extended these expressions within AUTOSTRUCTURE (Badnell 1997) for all multipoles. In figure 5, there should be a smooth transition from the final calculated reduced collision strength to the infinite energy point. There are some slight deviations from this ideal, but they will have a negligible effect on the Maxwell-averaged effective collision strengths.

Table 5 provides effective collision strengths from the ground state and first metastable term, giving a comparison between the results of our non-pseudostate model and our most elaborate pseudostate model. The effective collision strengths from our non-pseudostate R-matrix calculations are consistently higher than those from our RMPS calculations, but this tends to be most pronounced at intermediate temperatures. At lower electron energies, the effects of coupling to the target continuum are present, but are significantly smaller than at

Table 5. Collision strength comparisons between the non-pseudostate R-matrix model a (right-hand columns) and the $n = 11$ pseudostate model c (left-hand columns) from the ground-state and first metastable terms.

i	j	4×10^3 K		8×10^4 K		2×10^6 K		2×10^7 K	
1	2	1.36(−1)	1.39(−1)	6.83(−2)	7.74(−2)	1.38(−2)	1.64(−2)	2.65(−3)	3.11(−3)
1	3	4.76(−2)	5.87(−2)	3.69(−2)	4.85(−2)	5.43(−2)	7.43(−2)	8.27(−2)	9.63(−2)
1	4	8.15(−2)	9.36(−2)	8.32(−2)	9.53(−2)	3.49(−2)	4.70(−2)	7.56(−3)	1.02(−2)
1	5	3.34(−2)	3.55(−2)	5.27(−2)	6.56(−2)	3.26(−1)	4.02(−1)	9.17(−1)	1.03(+0)
1	6	2.62(−2)	2.90(−2)	1.26(−2)	1.69(−2)	3.16(−3)	4.19(−3)	6.08(−4)	7.56(−4)
1	7	9.01(−3)	1.10(−2)	7.00(−3)	1.24(−2)	1.17(−2)	1.92(−2)	1.93(−2)	2.50(−2)
1	8	1.24(−2)	1.92(−2)	1.56(−2)	2.21(−2)	8.22(−3)	1.21(−2)	1.85(−3)	2.58(−3)
1	9	4.53(−3)	5.62(−3)	4.16(−3)	5.39(−3)	1.18(−3)	1.43(−3)	2.26(−4)	2.58(−4)
1	10	6.10(−3)	7.50(−3)	5.00(−3)	7.17(−3)	5.33(−3)	6.28(−3)	7.13(−3)	7.51(−3)
1	11	4.22(−3)	5.71(−3)	9.80(−3)	1.80(−2)	7.11(−2)	1.06(−1)	2.04(−1)	2.57(−1)
1	12	6.23(−3)	9.45(−3)	4.45(−3)	7.92(−3)	1.24(−3)	1.75(−3)	2.37(−4)	2.81(−4)
1	13	3.01(−3)	4.72(−3)	2.51(−3)	6.62(−3)	4.68(−3)	8.72(−3)	8.19(−3)	1.11(−2)
1	14	5.28(−3)	7.53(−3)	5.47(−3)	1.01(−2)	3.07(−3)	4.94(−3)	6.93(−4)	1.02(−3)
1	15	2.33(−3)	2.83(−3)	1.95(−3)	3.18(−3)	6.60(−4)	8.16(−4)	1.31(−4)	1.49(−4)
1	16	1.41(−3)	1.82(−3)	5.97(−4)	6.99(−4)	5.69(−5)	6.17(−5)	6.86(−6)	7.15(−6)
1	17	1.55(−3)	2.04(−3)	5.86(−4)	7.87(−4)	1.08(−4)	1.50(−4)	5.84(−5)	6.48(−5)
1	18	3.28(−3)	3.77(−3)	2.27(−3)	4.64(−3)	2.87(−3)	3.54(−3)	3.77(−3)	3.96(−3)
1	19	1.71(−3)	1.93(−3)	3.50(−3)	9.89(−3)	2.96(−2)	4.81(−2)	9.17(−2)	1.13(−1)
2	3	1.51(+0)	1.41(+0)	6.92(−1)	7.15(−1)	1.18(−1)	1.27(−1)	2.12(−2)	2.21(−2)
2	4	2.65(+1)	2.64(+1)	4.46(+1)	4.78(+1)	1.10(+2)	1.14(+2)	1.62(+2)	1.67(+2)
2	5	6.94(−1)	6.94(−1)	5.96(−1)	6.37(−1)	8.52(−2)	1.09(−1)	1.13(−2)	1.43(−2)
2	6	2.23(+0)	1.98(+0)	1.38(+0)	1.37(+0)	1.98(+0)	1.94(+0)	2.15(+0)	2.03(+0)
2	7	2.49(−1)	2.27(−1)	7.01(−2)	7.99(−2)	7.29(−3)	1.01(−2)	1.03(−3)	1.38(−3)
2	8	9.14(−1)	1.18(+0)	8.66(−1)	8.99(−1)	3.74(+0)	3.70(+0)	8.30(+0)	8.41(+0)
2	9	1.03(+0)	1.10(+0)	1.74(+0)	2.12(+0)	4.99(+0)	5.60(+0)	6.19(+0)	6.48(+0)
2	10	2.54(−1)	2.59(−1)	1.72(−1)	2.22(−1)	2.37(−2)	3.93(−2)	3.17(−3)	4.83(−3)
2	11	1.02(−1)	1.05(−1)	8.67(−2)	1.01(−1)	1.23(−2)	1.77(−2)	1.56(−3)	2.21(−3)
2	12	3.63(−1)	3.47(−1)	2.48(−1)	2.88(−1)	3.61(−1)	3.06(−1)	3.80(−1)	2.94(−1)
2	13	5.15(−2)	5.39(−2)	1.99(−2)	3.20(−2)	2.23(−3)	4.44(−3)	2.97(−4)	5.60(−4)
2	14	3.17(−1)	3.41(−1)	2.96(−1)	4.12(−1)	7.94(−1)	9.49(−1)	1.23(+0)	1.70(+0)
2	15	2.37(−1)	2.64(−1)	3.13(−1)	5.97(−1)	9.72(−1)	1.22(+0)	1.27(+0)	1.34(+0)
2	16	2.28(−1)	2.62(−1)	2.31(−1)	3.21(−1)	2.89(−1)	3.22(−1)	2.78(−1)	2.91(−1)
2	17	6.57(−2)	7.46(−2)	3.03(−2)	4.25(−2)	3.28(−3)	5.28(−3)	3.93(−4)	5.97(−4)
2	18	1.02(−1)	9.93(−2)	5.18(−2)	9.57(−2)	7.85(−3)	1.67(−2)	1.12(−3)	2.04(−3)
2	19	4.39(−2)	3.78(−2)	3.22(−2)	4.89(−2)	4.63(−3)	8.73(−3)	5.93(−4)	1.06(−3)

energies above the ionization limit; thus, these differences are often not very large at low temperatures. The contributions to the dipole-allowed effective collision strength at high temperatures are dominated by high partial waves that are less susceptible to continuum coupling; hence, we have a gradual convergence in the effective collision strengths at high temperatures. This is exemplified by the $1s^2\ ^1S$–$1s4p\ ^1P$ transition (1–5), where at 4×10^3 K there is good agreement between models a and c, but this diverges by a factor of 2–3 by 8×10^4 K, before reaching agreement to within approximately 10% by 2×10^7 K. Although this trend in the variation of the effects of continuum coupling is also seen for some of the spin-allowed, non-dipole transitions, it is less pronounced in the spin-changing transitions since they fall off asymptotically with energy as E^{-2}.

The pseudostates not only act to approximate coupling to the high bound states and the continuum; through configuration interaction, they also affect the spectroscopic terms. Thus,

we have to be careful in attributing the differences in the effective collision strengths between models a and c solely to the effects of continuum coupling, as opposed to changes in the target structure. For example, the high-energy form of our effective collision strengths for dipole-allowed transitions is affected by the infinite-energy Bethe limits, which in turn are determined by the line strengths. Thus, we have examined the line strengths, both with and without the inclusion of pseudostates, to see if there were any large differences between models a and c. In the case of dipole excitations from the ground state, the line strengths differ by 12% for the $1s^2$–1s3p transition, while the collision strengths in the middle plot of figure 2 differ by about 90%, at 9 Ryd. For the $1s^2$–1s4p transition, for which there is the greatest sensitivity to continuum coupling, the line strengths differ by just over 1%, but the collision strengths in the bottom plot in figure 2 differ by about 140%, at 9 Ryd. On the basis of more complete comparisons of energies and radiative rates between these two models, we conclude that the differences between the effective collision strengths from models a and c are indeed primarily due to the effects of coupling to the target continuum.

Various transitions in Li^+ have different characteristics. For example, the first dipole-allowed transition from the ground state, having an energy separation of over 4 Ryd, is almost fully converged by $L = 11$ over the energy range at which these calculations were performed. Thus, the effective collision strengths for dipole-allowed transitions with larger threshold energies are quite sensitive to coupling effects, including coupling to the target continuum. On the other hand, the 1s4s–1s4p transition requires the inclusion of a top-up, in addition to our explicitly calculated partial-wave contributions through $L = 60$. These nearly degenerate dipole-allowed transitions rely almost entirely on the top-up procedure and the infinite-energy Bethe limit. Their collision strengths can exceed 1000 and ultimately the quality of the effective collision strengths for these transitions depends on the accuracy of the line strength. The non-dipole transitions, which tend to have much weaker background collision strengths, are often dominated by the resonance contributions (see, for example, figure 4). Their effective collision strengths are sensitive to coupling effects as well as the amount of correlation included within the $(N + 1)$-electron Hamiltonian; furthermore, in calculating the effective collision strengths for these transitions, significant effort must be made to fully resolve the dominant resonant structures.

The full set of results for energy levels, dipole radiative rates and effective collision strengths (including Born limits) over $T = 4 \times 10^3$–2×10^7 K, tabulated in the ADAS adf04 format (Summers 1994, 1999), is available via the Worldwide Web at http://www-cfadc.phy.ornl.gov/data_and_codes[5].

4. Conclusion

We have completed extensive RMPS calculations for the electron-impact excitation of Li^+. By comparing the results of our RMPS calculations with an *R*-matrix calculation without pseudostates, we have been able to demonstrate the large effects of coupling to the target continuum and high bound states in this ion. For example, at 8×10^4 K some of the effective collision strengths determined from our non-pseudostate calculation are more than a factor of two larger than the effective collision strengths determined from our most complete pseudostate calculation. Although there are differences between the collision strengths determined from our two pseudostate models, they are relatively small compared to the total effect of coupling to the target continuum; thus we would expect our largest RMPS calculation should be nearly converged with respect to the size of the pseudostate expansion.

[5] One of the authors (CPB) will be glad to provide all the effective collision strengths in electronic form to any interested readers (ballance@vanadium.rollins.edu).

It is very difficult to assess our results for all 171 transitions among the 19 terms included in this work. However, on the basis of the quality of the target states and the size of the pseudostate expansion included in our most extensive RMPS calculation, our effective collision strengths for the strong dipole-allowed transitions from the ground and metastable states should be accurate to approximately 15%. As discussed earlier, the effective collision strengths for those dipole-allowed transitions, involving small threshold energies, are dominated by top-ups and the infinite-energy Bethe limits; thus, their accuracy depends on the quality of the target wavefunctions.

For the non-dipole transitions, that can be dominated by resonance contributions, it is nearly impossible to assess the accuracy of the effective collision strengths. However, the resonances are completely resolved by the energy mesh that we employed and the effects of coupling have been accurately included in our largest RMPS calculation. Nevertheless, there is always uncertainty associated with the size and position of the dominant resonance structures, which will affect the effective collision strengths most at low temperatures.

Now that we have completed a benchmark calculation for this ion, future studies will be performed to determine the methods by which we might be able to generate a reduced pseudostate basis and still achieve the same degree of accuracy in the effective collision strengths. One approach would be to use a smaller, but optimized, set of pseudostates. Another possibility would be to include a full set of pseudostates within our configuration–interaction expansion, but gradually reduce the number of higher energy states included in our CC expansion. If such reduced pseudostate methods cannot be developed, the inclusion of continuum coupling effects in more complex species will become prohibitively large, even with the use of massively parallel computers.

A complete excitation data set for isonuclear Li has now been completed. In conjunction with ionization and recombination rate co-efficients, these data should contribute significantly to current fusion diagnostic and modelling. For example, at the DIII-D experiment, Li is inserted into the tokamak via a probe; the resulting transport and subsequent ionization monitored at various points as the Li penetrates the core can be compared with modelling our data.

Acknowledgments

In this work, CPB was supported by a US DoE SciDAC grant (DEFG02-01ER54G44) to Auburn University, DCG was supported by a US DoE Grant (DE-FG02-96-ER54367) and DMM was supported by a subcontract with Los Alamos National Laboratory.

References

Anderson H, Ballance C P, Badnell N R and Summers H P 2000 *J. Phys. B: At. Mol. Opt. Phys.* **33** 1255–62
Badnell N R 1997 *J. Phys. B: At. Mol. Opt. Phys.* **30** 1–11
Badnell N R and Gorczyca T W 1997 *J. Phys. B: At. Mol. Opt. Phys.* **30** 2011–9
Bartschat K 1998 *J. Phys. B: At. Mol. Opt. Phys.* **31** L469–76
Bartschat K and Bray I 1997 *J. Phys. B: At. Mol. Opt. Phys.* **30** L109–14
Bartschat K, Hudson E T, Scott M P, Burke P G and Burke V M 1996 *J. Phys. B: At. Mol. Opt. Phys.* **29** 115–23
Berrington K A, Eissner W B and Norrington P H 1995 *Comput. Phys. Commun.* **92** 290–420
Berrington K A and Nakazki S 1991 *J. Phys. B: At. Mol. Opt. Phys.* **24** 1411–21
Brown G J N, Scott M P and Berrington K A 1999 *J. Phys. B: At. Mol. Opt. Phys.* **32** 737–48
Burgess A 1974 *J. Phys. B: At. Mol. Phys.* **7** L364–7
Burgess A, Chidichimo M C and Tully J A 1997 *J. Phys. B: At. Mol. Opt. Phys.* **30** 33–57
Burgess A, Hummer D G and Tully J A 1970 *Phil. Trans. R. Soc.* A **266** 225–79
Burgess A and Tully J A 1992 *Astron. Astrophys.* **254** 436–53

Burke V M, Burke P G and Scott N S 1992 *Comput. Phys. Commun.* **69** 76–98
Christensen R B and Norcross D W 1984 *Phys. Rev.* A **31** 142–51
Griffin D C, Badnell N R and Pindzola M S 2000 *J. Phys. B: At. Mol. Opt. Phys.* **33** 1013–28
Griffin D C and Pindzola M S 1990 *Phys. Rev.* A **42** 248–54
Marchalant P J, Bartschat K and Bray I 1997 *J. Phys. B: At. Mol. Opt. Phys.* **30** L435–40
Mitnik D M, Griffin D C and Badnell N R 2001 *J. Phys. B: At. Mol. Opt. Phys.* **34** 4455–73
NIST webpage http://physics.nist.gov/cgi-bin/AtData/main_asd
Seaton M J 1983 *Rep. Prog. Phys.* **46** 168–257
Summers H P 1994 *JET Joint Undertaking Report* JET-IR(94)06
Summers H P 1999 *ADAS User Manual Version 2.1* webpage http://adas.phys.strath.ac.uk
Whiteford A D, Badnell N R, Ballance C P, O'Mullane M G, Summers H P and Thomas A L 2001 *J. Phys. B: At. Mol. Opt. Phys.* **34** 3179–91